

# Supersymmetrically bounding of asymmetric states and quantum phase transitions by anti-crossing of symmetric states

Muhammad Imran Afzal<sup>1</sup>, Hoonsoo Kang<sup>1\*</sup> and Yong Tak Lee<sup>1,2\*</sup>

<sup>1</sup>Advanced Photonics Research Institute, Gwangju Institute of Science and Technology, Gwangju 500-712, Korea.

<sup>2</sup>School of Information and Communications, Gwangju Institute of Science and Technology, Gwangju, 500-712, Korea.

[imran@gist.ac.kr](mailto:imran@gist.ac.kr)

\*[hunskang@gist.ac.kr](mailto:hunskang@gist.ac.kr)

\*[ytlee@gist.ac.kr](mailto:ytlee@gist.ac.kr)

Von Neumann and Wigner theorized bounding of asymmetric eigenstates and anti-crossing of symmetric eigenstates. Experiments have shown that owing to anti-crossing and similar radiation rates, graphene-like resonance of inhomogeneously strained photonic eigenstates can generate pseudomagnetic field, bandgaps and Landau levels, while dissimilar rates induce non-Hermiticity. Here, we showed experimentally higher-order supersymmetry and quantum phase transitions by resonance between similar one dimensional lattices. The lattices consisted of inhomogeneously strain-like phases of triangular solitons. The resonance created two dimensional inhomogeneously deformed photonic graphene. All parent eigenstates are annihilated. Where eigenstates of mildly strained solitons are annihilated with similar (power law) rates through one tail only and generated Hermitianally bounded eigenstates. The strongly strained solitons, positive defects are annihilated exponentially through both tails with dissimilar rates. Which bounded eigenstates through non-Hermitianally generated exceptional points. However, negative defects were effectively amplified. Supersymmetry is evident with preservation of shapes and relative phase differences of parent solitons. Localizations of energies generated from annihilations of mildly and strongly strained soliton's eigenstates were responsible for geometrical (Berry) and topological phase transitions, respectively. Both contributed to generate quantum Zeno phase, while only strong twists generated dynamic localization. Anti-bunching-like condensation was also observed.

The theory of supersymmetry (SUSY) describes duality between bosons and fermions. Since our present living environment does not allow any SUSY phenomenon therefore according to the original theory, if SUSY exists, it needs to be broken symmetry<sup>1-2</sup>. The confirmation of the original SUSY is still unsuccessful in the initial rounds of the Large Hadron Collider experiments. However, SUSY techniques have been proved helpful for finding powerful methods for approximation and shape invariance<sup>3</sup>. One of the most important application is quantum information processing or quantum simulation because of robustness against decoherence and dissipation. However, with the advent of Witten-index's non-zero value (all parent eigenstates must be annihilated)<sup>4</sup>, unbroken SUSY could be observable in table top quantum and dissipative systems<sup>5</sup> e.g. optics, semiconductor and condensed matter systems.

Dirac cones are Hermitian system and governs the intriguing properties of graphene<sup>6</sup>, topological insulators<sup>7</sup> and configured condensed matter systems<sup>8</sup>. In optics, electronic graphene-like resonant Dirac cones<sup>9-10</sup> can be realized by resonance of degenerate photonic states at the Brillouin zone. This leads to a linear Dirac dispersion owing to the anti-crossing<sup>11</sup> of symmetric photonic states<sup>12</sup>. Which is clearly observable in case of topological insulators as bulk states bandgaps<sup>13</sup>. In case of inhomogeneous strained waveguide arrays, the resonance leads to pseudomagnetic field and isolated landau levels<sup>14</sup>, where level spacing is unique to the corresponding lattice.

Non-Hermitian systems are distinguished from Hermitians by exhibiting Exceptional Points (EPs). Which abruptly coalesce the eigenmodes without any threshold barrier<sup>15</sup>. The EP is a point of confusion in Hermitian system due to sudden change, which give rise imaginary potential. For example sudden loss induced counter intuitive observations at exponential transition rates such as lasing<sup>16-18</sup> and unidirectionality<sup>19-25</sup>. Topologies of EPs are investigated in acoustics<sup>26</sup> and microwave systems<sup>27-29</sup>. Connection between Dirac cones and EPs and their dynamics have been theoretically investigated in photonic honeycomb lattices<sup>30-33</sup>. However, a recent experiment demonstrates EPs in a honeycomb via dissimilar radiation rates. The EPs deform the Dirac cones into lantern-like shape<sup>34</sup>.

Here we experimentally demonstrated that owing to anti-crossing in photonic graphene-like resonance leads to Hermitian and non-Hermitian bounding of eigenstates. Hermitian and non-Hermitian bounding is due to similar and dissimilar (non-Hermitian) radiation-loss rates from the resonant cones, respectively. In these transformations the SUSY i.e., relative gaps of eigenstates and shapes of parent solitons remained intact, therefore we named supersymmetric bounding of states. These observations have no exact experimental analogue.

We considered a soliton with phase  $\varphi_i$  as mildly twisted when  $\varphi_{i+1} - \varphi_i > 0$  and  $\varphi_i - \varphi_{i-1} > 0$ , while  $|\varphi_{i+1} - \varphi_i| \neq |\varphi_i - \varphi_{i-1}|$ . A soliton with phase  $\varphi_i$  is treated as strongly twisted when  $\varphi_{i+1} - \varphi_i < 0$  and  $\varphi_i - \varphi_{i-1} > 0$  or  $\varphi_{i+1} - \varphi_i > 0$  and  $\varphi_i - \varphi_{i-1} < 0$ . Former solitons are positive defects and later are negative defects. This description is represented schematically in Fig. 1(a) and Fig. 2(a). Owing to graphene-like resonance, mildly inhomogeneous strained-like modulation of phases  $\varphi_i$  of the soliton lattices generated similar pseudomagnetic flux  $\Phi$  owing to similar radiation rates, without undergoing the interband photonic transitions (evanescent tunnelling). The direction of the flux is opposite to y-axis. Due to similar radiation rate losses, all the eigenstates are annihilated with similar rates in the same direction. In our experiment the vector potential under the strain<sup>14</sup> can be described as  $A(r) = [\varphi_i]$  and pseudomagnetic field as  $B(r) = \nabla \times A(r)$ . However, strong twists with positive defects generated abruptly strong fluxes i.e., much greater than the mildly twist-induced pseudomagnetic field owing to dissimilar and exponential radiation rates. The dissimilar and exponential radiation rates induced EPs. Thus at EPs pseudomagnetic field rise exponential. In this case, the direction of the flux or radiation is orthogonal (parallel to x-axis) to the magnetic flux  $\Phi$  of mildly twisted solitons. This type of strong or non-Hermitian twists was never studied before. However, the slight dissimilarity<sup>34</sup> of exponential radiation rates caused to form spawning of EPs, which bounded both side eigenstates. Hermitian and non-Hermitian bounds are depicted in Fig. 1 (b) and 2 (b) with vertical black and red lines. The radiated energy from mildly and strongly twisted (positive defects) solitons localized as continuum without leaving its lattice, which is responsible for quantum phase transitions i.e., Berry and topological phases. Two localizations of radiated energies i.e., one part of the continuum along X-axis due to Hermitian and other part along Y-axis

due to EPs revealed as Zeno phase. While localized energies along X-axis due to only EPs gave dynamic localization and effective amplification. In Fig. 1 and 2 the continuums are symbolically represented with blue color filled rectangular boxes. (for detail see the text). However, we can imagine that in the presence of only mildly twisted solitons i.e., absence of the non-Hermiticity, only Berry (geometrical) phase<sup>34-36</sup> can be observed.

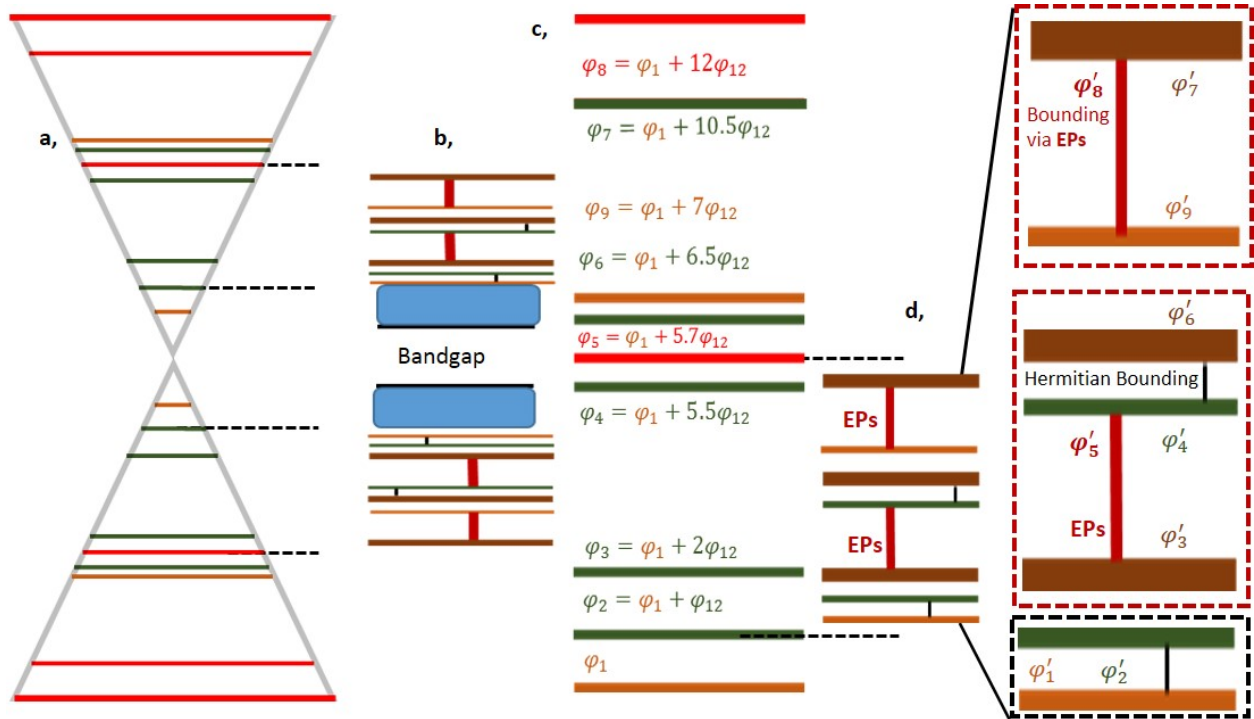


**Figure 1 | Supersymmetry, bounding of eigenstates and phase transitions through anti-crossing of mildly and strongly twisted nine parent eigenstates.** **a**, Graphene-like resonance of parent eigenstates. Where orange, green and red lines are eigenstates of boundary, mildly and strongly twisted (positive defect) soliton eigenstates, respectively. **b**, All parent eigenstates  $\varphi_i$  are annihilated and new (supersymmetric) eigenstates  $\varphi'_i$  confined between the parent region of eigenstates  $\varphi_2$  and  $\varphi_3$ . Due to anti-crossing between symmetric eigenstates (two cones) bandgaps and supersymmetric bounding generated. Where mildly twisted solitons decay by radiating similar rates and bounded Hermitianally (vertical black lines in **b** and **d**). While strongly twisted solitons vanished completely by decaying through exponential and dissimilar rates. This generated

spawning of EPs (vertical bold red lines) and bounded neighbouring eigenstates. Owing to EPs induced bounding, the bounded eigenstates are become boundary eigenstates. Which are shown with dark orange lines. The energies released from annihilations localized within the respective lattices as continuums. Which are symbolically represented with rectangular box filled with light blue color. The continuums controlled quantum phase transitions (see text for details). **c** and **d** are zoomed presentations of **a** and **b**. In **d**, red and black dotted rectangular boxes are drawn to explicitly show the non-Hermiticity and Hermiticity induced bound states.

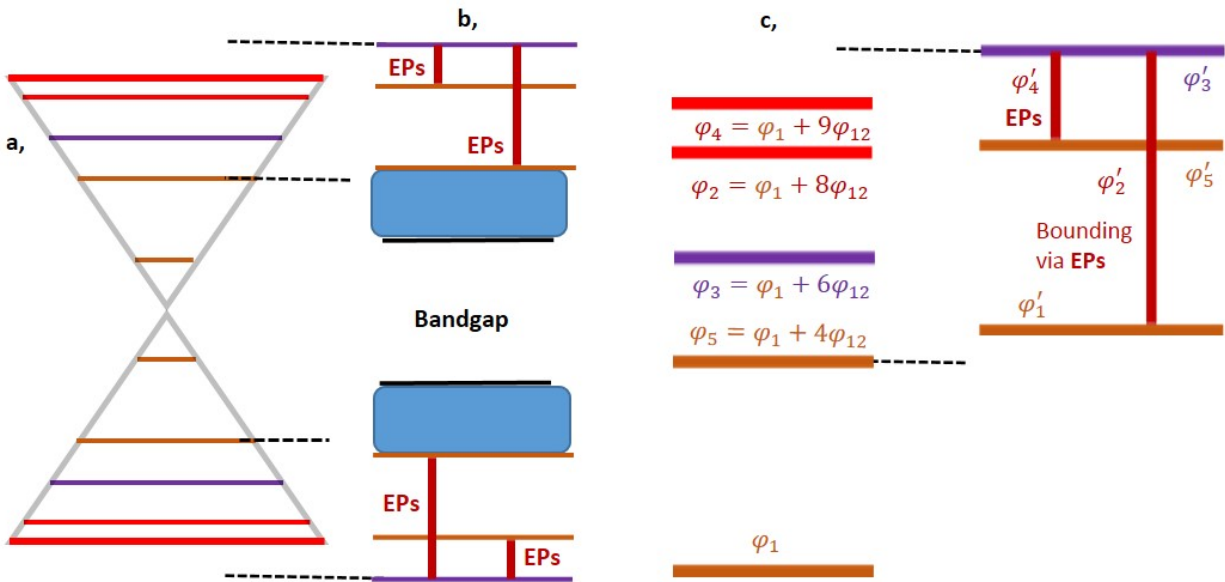


**Figure 2 | Supersymmetry, bounding of eigenstates and phase transitions through anti-crossing of strongly twisted five parent eigenstates.** **a**, Anti-crossing between five asymmetric parent eigenstates. Where orange, purple and red lines are eigenstates of boundary, two types of strongly twisted i.e., negative defect and positive defect soliton eigenstates. **b**, All parent eigenstates  $\varphi_i$  are annihilated. Most part of the spectrum of supersymmetric eigenstates  $\varphi'_i$  confined between the parent region of eigenstates  $\varphi_2$  and  $\varphi_5$ , however, supersymmetric eigenstate  $\varphi'_3$  is beyond the region of parent spectrum. Due to anti-crossing between symmetric eigenstates (two cones) bandgaps and supersymmetric bounding generated. Where negative defect, strongly twisted soliton retained its parent eigenstate and therefore appeared as effectively amplified. While second type of strongly twisted solitons, positive defects vanished completely by decaying through exponential

and dissimilar rates. This generated spawning of EPs (vertical bold red lines) and bounded neighbouring eigenstates. Owing to EPs induced bounding, the bounded eigenstates are become boundary eigenstates. Which are shown with dark orange lines. The energies released from annihilations localized within the respective lattices as continuum. Which is shown with rectangular box filled with light blue color. Here the continuum is only responsible for topological quantum phase transition. Due to absence of mildly twisted solitons no berry phase can be observed (see text for details). **c** is zoomed presentations of **a** and **b**.

The experimental setup is shown in Fig. 3. The two soliton lattices occupying wavelength range from 999.5 to 1,009.5 nm are entered in two metre loop of optical fiber. After meeting with first coupler, two similar copies are generated owing to power splitting. The optical spectrum of the lattices detected at the output of second coupler is captured using optical spectrum analyser (OSA). The lattices detected without any change in the structure due to absence of interference/resonance at the second coupler and shown in Fig. 4(a, c). As we can see in the Figure that the detected peak powers of the lattices are 3.38 and 1.15, respectively. The first lattice consisted of nine solitons, where two are strongly twisted. Graphene-like resonance between the splitted lattices is achieved by resonances of the lattices at the second coupler by exactly matching the length of the two arms of the loop as shown in Fig. 3.

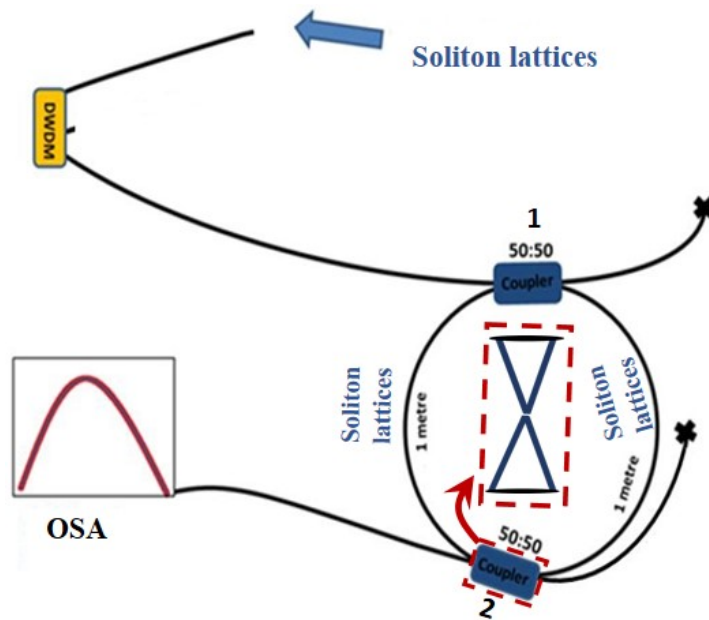


**Figure 3 | Experimental configuration.** The two soliton lattices having wavelength range from 999.5 to 1,009.5 nm are entered in two metre loop of optical fiber through the fibre dense wavelength division multiplexer (DWDM). The entire loop consists of a normal dispersion optical fibre (HI 980). The fibre exhibits zero dispersion at 1,300 nm, and the dispersion values at 980 nm are approximately -63 ps/nm/km. The fibre exhibited multimode character. Normal dispersion fiber is used to avoid modulation instability. Two copies of the input lattices with attenuated power are generated after meeting with the first 50:50 coupler. The optical spectrum of the lattices detected at the output of second coupler is captured using optical spectrum analyser (OSA). First the lattices are detected without any change in the structure due to absence of interference/resonance at the second coupler and shown in Fig. 4(a, c). Graphene-like resonance between the splitted lattices is achieved by resonances of the lattices at the second coupler by exactly matching the length of the two arms of the loop as shown in the figure. The inset is drawn to show the graphene-like resonance.

Supersymmetrically bounded eigenstates and quantum phase transitions generated from the resonance is shown in Fig. 4(b, d). A mode between the two lattices at  $\sim 1006$  is unaffected by the supersymmetric transformations. Which indicates the isolation between two lattices. Seemingly, this also shows that the supersymmetric transformation could not be produced in case of resonance of single soliton mode or eigenstate. Therefore presence of more than one modes in one wave packet is required to achieve graphene-like resonance. Eigenstates of soliton lattices detected at the output of the experimental setup without resonance is shown in Fig. 4(a) and c. First and second parent lattice are consisted of nine and five eigenstates ( $\varphi_i$ ), respectively. Where first lattice contains two strongly twisted solitons, positive defects and second lattice contains positive defect and one negative defect solitons, as shown in Fig. 4(a) and (c), respectively. After the resonance of each of the lattices with itself, supersymmetrically bounded eigenstates are observed. For the first and the second lattice is shown in Fig. 4(c) and (d), respectively. Where supersymmetric eigenstates are represented with  $\varphi'_i$ . On resonance mildly twisted solitons radiate through one tail only with similar radiation rates. Which generated Hermitian bounding while strongly twisted soliton with positive defect radiate through both tails with dissimilar rates and non-Hermitianally bounded the surrounding eigenstates. However the negative defect do not radiate which is probably due to its existence in between two positive defects.

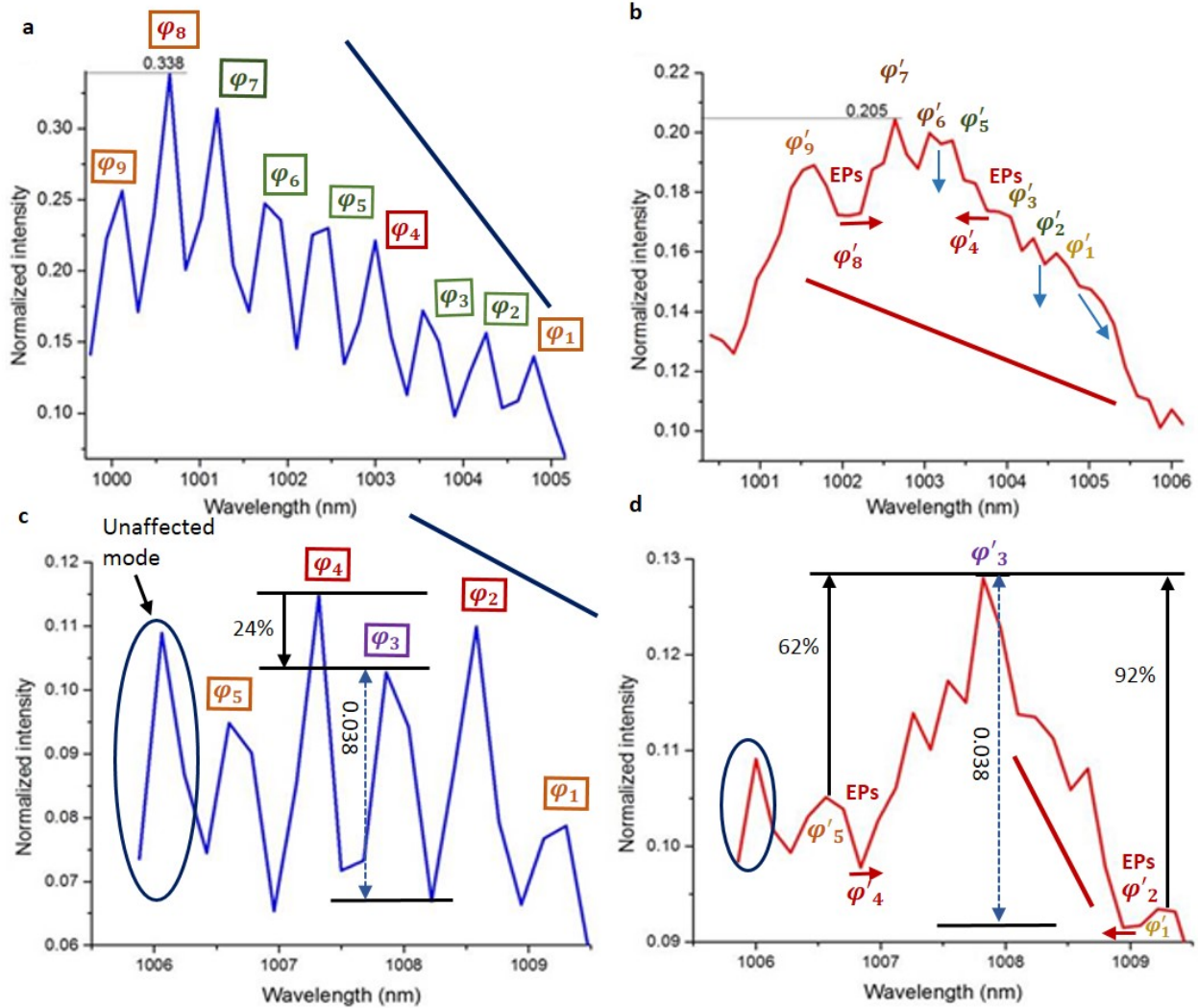


**Figure 4 | Eigenstates of soliton lattices detected at the output of the experimental setup, before and after generation of supersymmetric bounding of eigenstates, and effective amplification. a, c,** First and second parent lattice are consisted of nine and five eigenstates ( $\varphi_i$ ), respectively. (for detail see Fig. 1 and 2 ). **c,** In this case the parent lattice (c) did not contain any Hermitian soliton however contained two types of strong twists i.e., both positive and negative defects. **b,** Supersymmetric eigenstates ( $\varphi'_i$ ) and their Hermitian and non-Hermitian bounding. Thin blue arrows are drawn to show the direction of radiation loss of Hermitian solitons. Thick red arrows indicate directions of the radiation owing to non-Hermiticity. All parent eigenstates of Hermitian solitons are annihilated and generated supersymmetric eigenstates ( $\varphi'_i$ ). Which are bounded Hermitianly. However, strongly twisted, positive defect solitons  $\varphi_4$  and  $\varphi_8$  are annihilated with exponential

and dissimilar rates, and vanished completely, while their positions remained localized,  $\varphi'_4$  and  $\varphi'_8$ . The non-Hermitian annihilation generated spawning of EPs, which bounded both side eigenstates. The peak power is reduced to 2.04  $\mu\text{W}$ . Instead of escaping, owing to pseudomagnetic field, the energies released by the annihilations localized to form a continuum and responsible for quantum phase transitions. The continuum decrease the slope of parent spectrum from 1.31 to 0.43. New slope is highlighted by the straight red line. This decrease in the slope of the redistributed eigenspectrum is interpreted as the quantum Zeno phase. The topological phase features are due to EPs while geometrical phase features are due to Hermiticity. **d**, In this case only non-Hermitian but very different dynamics are observed for negative defect soliton ( $\varphi'_3$ ), which sustain its parent energy 0.038 while surrounded by positive defects-induced EPs on both sides. Thus the defect with phase  $\varphi'_3$  appeared as effectively amplified. However, overall the spectrum of the eigenstates were dynamically localized due to localization of continuum along Y-axis. Which is evident with the increase in the slope from 0.54 to 1.91; these slopes are represented by blue (c) and red straight lines, respectively. A mode represented as ‘unaffected mode’ located at  $\sim 1006$  nm wavelength in **c**, and **d**, is unaffected by the transformations. Which indicates the isolation of first and second lattice from each other.

For the former the radiated energy accumulated along X-axis to form flat-band-like continuum<sup>14,34,37</sup> while in the later case the energy is accumulated along Y-axis. Former responsible for geometrical phase transition while later topological phase transition. Combination of geometrical and topological phase transitions enabled the observation of quantum Zeno phase as shown in Fig. 4(b). The non-Hermitian annihilations generated spawning of EPs, which bounded both side eigenstates. The peak power is reduced to 2.04  $\mu\text{W}$ . Here, the localizations of one part of the continuum along X-axis due to Hermitian and other part along Y-axis (at the bottom of  $\varphi'_5$ ,  $\varphi'_6$  and  $\varphi'_7$ ) due to EPs revealed as Zeno phase. The collective effect is represented with decrease in slope from 1.31 to 0.43, which are shown with blue and red straight lines in Fig. 4(a) and (b), respectively. While presence of a negative defect in between positive defects enabled the observation of dynamic localization of whole of the spectrum. Here localization of energies at the bottom of  $\varphi'_3$  revealed as dynamic localization and their parent and final slopes are represented with blue and red straight lines in Fig.

4(c) and (d), respectively. Contrary to positive defect, instead of radiating, negative defect was effectively amplified. The slope of parent spectrum increased from 0.54 to 1.91. This observation allows us to introduce an interesting postulate: if a SUSY potential could not preserve the eigenspectrum of the parent system in a specific dimension, then it will localize the eigenspectrum of parent potential to another dimension to obey the SUSY. This aspect is also important for understanding the increase and decrease in (effective) dimensions in any local system or evolution (growth) of new dimensions in a system including biology. In both of Fig. 4(b) and (d), the parent shapes of the solitons and their phase (spacing) difference are relatively preserved except positive defects. Or simply parent eigenstates  $\varphi_i$  are relatively preserved  $\varphi'_i$ . Therefore the bounded states are considered as supersymmetrically bounded states.

Our observed dynamic localization is different from the conventional Anderson localization in optics; however, the shapes are in agreement with Anderson localization<sup>38</sup> and the anti-Zeno effect<sup>39-40</sup> in condensed matter and effective amplification<sup>41</sup> in quantum optics. Effective amplification is a necessary element for experimental implementation of quantum computation, quantum detection and Schrodinger's cat-based amplification of the quantum states. A comparison of Figs. 4(c) and (d) in terms of the effective amplification of modes instead of the redistribution of the energies of the parent eigenstates demonstrates that the mode at 1,007.86 nm is amplified from 0.103 to 0.128, and the effective amplification ranges from -24% (as indicated by the black downward arrow) to 62% and 92% (as indicated by black upward arrows). The relative power (0.038) of the signal at 1,007.86 nm is nearly the same for the parent and SUSY transformed system.

Redistribution of energies in the localized continuums allowed us to observe the reduced intensity fluctuations in original SUSY systems as shown in Fig. 4(b) and (d) as well as in ascending power distribution of continuums, as shown in Fig. 5. Which is analogous to anti-bunched clustering. In particular, redistributed energies in the quantum Zeno phase profile (distribution of red circles in Fig. 5(a)) clearly show antibunched photonic bands or clustering of the states. Indeed, theoretical study of supersymmetrically generated photonic bands in disordered optical potentials (waveguide arrays) without anti-crossing was reported in a recent paper<sup>42</sup>. However, in principle our results reported in the present manuscript are different.

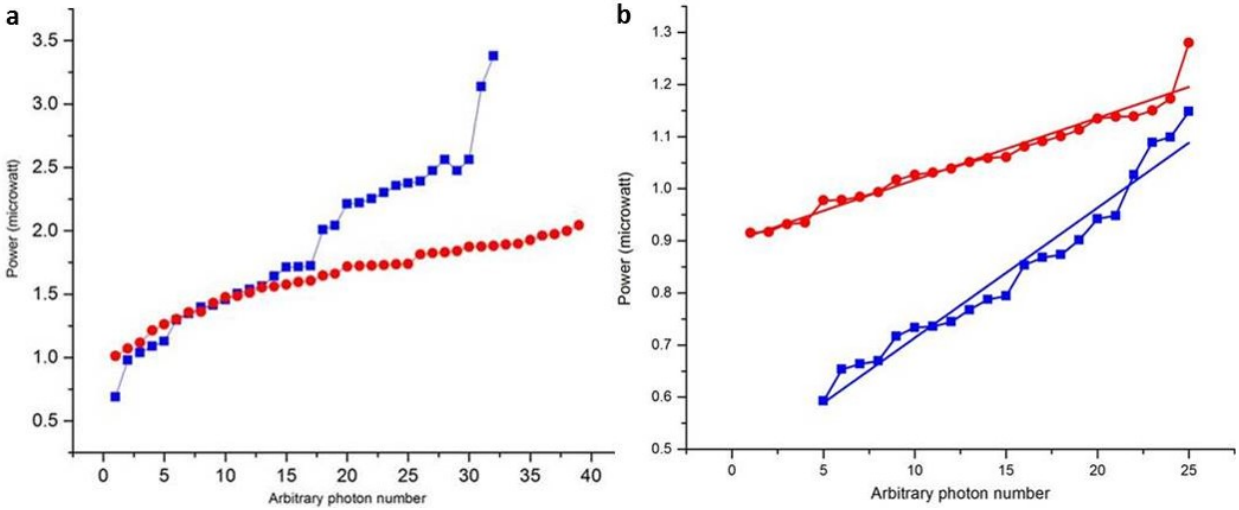


**Figure 5 | Comparison of the ascending power distribution of continuums of parent soliton lattices, Fig. 4(a) and Fig. 4(c) with the continuums of SUSY bounded lattices, Figs. 4(b) and 4(b).** **a**, The power for an arbitrary number of photons in the first parent lattice is shown in blue, and the power redistribution in SUSY lattice is shown in **red**. This shows formation of three clusters. Interestingly, Fig. 4(b) also shows three bounds. **b**, The power for an arbitrary number of photons in second parent lattice is shown in blue, and the power redistribution in SUSY lattice is shown in red. The Fig. 4(d) shows two boundings, however, due to negative defect, even the presence of two boundings formed a single lattice like structure. The similarity between the behaviour of Fig. 4 and 5 could be understood by considering the localisation of the energies in the continuum as represent with lines with slopes in Fig. 4(b, d).

### Conclusion and summary

We observed supersymmetrically bounded eigenstates through Hermiticity and non-Hermiticity in soliton lattices having weakly and strongly twisted solitons or inhomogeneous eigenstates. Which was achieved by anti-crossing of asymmetric states. This might be possible that the non-Hermiticity or abruptly annihilations of few modes in a lattice of very large number of Hermitian modes could play a crucial role in quantum phase transitions. Where the Hermitian modes are only responsible for Berry phase. Preservation of parent shapes and phase difference of the solitons are clear evidence of SUSY. While large number of annihilations of parent

eigenstates is an evidence of the higher-order transformations. Different topologies of the EPs are also observed, where some are matched with spawning of EPs in photonic graphene<sup>34</sup> and other with EPs in acoustics<sup>26</sup> and microwave billiards<sup>27-29</sup>. We believe the results will prove very helpful to envision strongly bounded eigenstates via non-Hermiticity beyond the Von Neumann and Wigner's Hermitianly bounded states. Seemingly, our results may also be visualized as Hermitian<sup>14</sup> and non-Hermitian bounding of Landau levels.

## References

1. Martin, S. P. A Supersymmetry primer' in: 'Perspectives in Supersymmetry. G.L. Kane (Ed.), World Scientific, Singapore, and arXiv:9709356 [hep-ph].
2. Dine, M. Supersymmetry and String Theory: Beyond the Standard Model (Cambridge University Press, 2007).
3. Cooper, F., Khare, A. & Sukhatme, U. Supersymmetry and quantum mechanics. *Phys. Rep.* **251**, 267 (1995).
4. Witten, E. Constraints on Supersymmetry Breaking. *Nucl. Phys.* **B202**, 253-316 (1982).
5. Tomka, M., Pletyukhov, M., & Gritsev, V. Supersymmetry in quantum optics and in spin-orbit coupled systems. *Sci. Rep.* **5**, 13097 (2015).
6. Castro Neto, A. H., Guinea, F., Peres, N. M. R., Novoselov, K. S. & Geim, A. K. The electronic properties of graphene. *Rev. Mod. Phys.* **81**, 109–162 (2009)
7. Hasan, M. Z. & Kane, C. L. Colloquium: topological insulators. *Rev. Mod. Phys.* **82**, 3045 (2010)
8. Tarruell, L., Greif, D., Uehlinger, T., Jotzu, G. & Esslinger, T. Creating, moving and merging dirac points with a fermi gas in a tunable honeycomb lattice. *Nature* **483**, 302–305 (2012).

9. Kane, C. L. & Mele, E. J. Size, Shape, and Low Energy Electronic Structure of Carbon Nanotubes. *Phys. Rev. Lett.* **78**, 1932–1935 (1997).
10. Zhang, Y., Tan, Y.-W., Stormer, H. L. & Kim, P. Experimental observation of the quantum Hall effect and Berry's phase in graphene. *Nature* **438**, 201–204 (2005).
11. Von Neumann, J. & Wigner, E. Über merkwürdige diskrete Eigenwerte. *Phys. Z.* **30**, 465–467 (1929).
12. Sakoda, K. Proof of the universality of mode symmetries in creating photonic dirac cones. *Opt. Express* **20**, 25181–25194 (2012).
13. Rechtsman, M. C. et al. Photonic Floquet topological insulators. *Nature* **496**, 196–200 (2013).
14. Rechtsman, M. C. et al. Strain-induced pseudomagnetic field and photonic landau levels in dielectric structures. *Nature Photon.* **7**, 153–158 (2013).
15. Heiss, W. The physics of exceptional points. *J. Phys. A* **45**, 444016 (2012).
16. Liertzer, M. et al. Pump-induced exceptional points in lasers. *Phys. Rev. Lett.* **108**, 173901 (2012).
17. Brandstetter, M. et al. Reversing the pump-dependence of a laser at an exceptional point. *Nature Comm.* **5**, 4034 (2014).
18. Peng, B. et al. Loss-induced suppression and revival of lasing. *Science* **346**, 328–332 (2014).
19. Guo, A. et al. Observation of PT-symmetry breaking in complex optical potentials. *Phys. Rev. Lett.* **103**, 093902 (2009).
20. Makris, K., El-Ganainy, R., Christodoulides, D. & Musslimani, Z. H. Beam dynamics in PT symmetric optical lattices. *Phys. Rev. Lett.* **100**, 103904 (2008).
21. Longhi, S. Bloch oscillations in complex crystals with PT symmetry. *Phys. Rev. Lett.* **103**,

123601 (2009).

22. Lin, Z. et al. Unidirectional invisibility induced by PT-symmetric periodic structures. *Phys.*

*Rev. Lett.* **106**, 213901 (2011).

23. Feng, L. et al. Experimental demonstration of a unidirectional reflectionless parity-time metamaterial at optical frequencies. *Nature materials* **12**, 108–113 (2013).

24. Peng, B. et al. Parity-time-symmetric whispering-gallery microcavities. *Nature Physics* **10**, 394–398 (2014).

25. Chang, L. et al. Parity-time symmetry and variable optical isolation in active-passive-coupled microresonators. *Nature Photon.* **8**, 524–529 (2014)

26. Ding, K. et al. The emergence, coalescence and topological properties of multiple exceptional points and their experimental realization. arXiv:1509.06886 (2015).

27. Dembowski, C. et al. Experimental Observation of the Topological Structure of Exceptional Points. *Phys. Rev. Lett.* **86**, 787 (2001).

28. Dembowski, C. et al. Observation of a Chiral State in a Microwave Cavity. *Phys. Rev. Lett.* **90**, 034101 (2003).

29. Lee, S-Y. et al. Geometric phase around multiple exceptional points. *Phys. Rev. A* **85**, 064103 (2012).

30. Szameit, A. P T-symmetry in honeycomb photonic lattices. *Phys. Rev. A* **84**, 021806 (2011).

31. Ramezani, H. Kottos, T. Kovanis, V. & Christodoulides, D. N. Exceptional-point dynamics in photonic honeycomb lattices with PT symmetry. *Phys. Rev. A* **85**, 013818 (2012).

32. Yannopoulos, V. Spontaneous PT-symmetry breaking in complex frequency band structures. *Phys. Rev. A* **89**, 013808 (2014).
33. Monticone, F. & Alu, A. Embedded photonic eigenvalues in 3d nanostructures. *Phys. Rev. Lett.* **112**, 213903 (2014).
34. Zhen, B., Hsu, C. W., Igarashi, Y., Lu, L., Kaminer, I., Pick, A., Chua, S.-L., Joannopoulos, J. D. & Soljacic, M. Spawning rings of exceptional points out of Dirac cones. *Nature* **525**, 354 (2015).
35. Chan, C., Hang, Z. H. & Huang, X. Dirac dispersion in two-dimensional photonic crystals. *Adv. Optoelectron.* **2012**, 313984 (2012).
36. Mei, J., Wu, Y., Chan, C. & Zhang, Z.-Q. First-principles study of Dirac and Dirac-like cones in phononic and photonic crystals. *Phys. Rev. B* **86**, 035141 (2012).
37. Huang, X., Lai, Y., Hang, Z. H., Zheng, H. & Chan, C. Dirac cones induced by accidental degeneracy in photonic crystals and zero-refractive-index materials. *Nature materials* **10**, 582–586 (2011).
38. Roati, G. et al. Anderson localization of a non-interacting Bose-Einstein condensate. *Nature* **453**, 895–898 (2008).
39. Fischer, M. C., Gutiérrez-Medina, B. & Raizen, M. G. Observation of the quantum Zeno and anti-Zeno effects in an unstable system. *Phys. Rev. Lett.* **87**, 040402-040404 (2001),
40. Fujii, K. & Yamamoto, K. Anti-Zeno effect for quantum transport in disordered system. *Phys. Rev. A* **82**, 042109 (2010).
41. Zavatta, A., Fiurauskas, J. & Bellini, M. A high-fidelity noiseless amplifier for quantum light states. *Nature Photon.* **5**, 52–60 (2010).

42. Yu, S., Piao, X., Hong, J. & Park, N. Bloch-like waves in random-walk potentials based on supersymmetry. *Nature Comm.* **6**, 8269 (2015).

### **Acknowledgements**

This work was partially supported by the “Systems biology infrastructure establishment grant” and the “Ultrashort Quantum Beam Facility Program” through a grant provided by the Gwangju Institute of Science and Technology in 2015.

### **Author Contributions**

M.I. conceived the idea, designed and performed the experiments and the analysis of results. Y.T. provided insightful advice and encouraged M.I. for the investigation and supervised the project. M.I., H.S. and Y.T. wrote the manuscript. All authors reviewed the manuscript.

### **Competing Interests Statement**

The authors declare that they have no competing financial interests.